

Analysis of Impedance and Admittance Data for Solids and Liquids

J. Ross Macdonald* and J. A. Garber¹

Department of Physics and Astronomy, University of North Carolina, Chapel Hill, North Carolina 27514

ABSTRACT

Some problems of analyzing small-signal impedance data on solids or liquids are discussed. A method of using ordinary nonlinear least squares fitting procedures with minor modification to fit at the same time real and imaginary functions of the same set of unknown parameters to complex data is described in detail. This method of complex least squares fitting, which has several advantages over previous approaches, is illustrated by fitting equivalent circuit impedances to some polycrystalline β -alumina impedance data and to synthetic impedance and admittance data calculated from a theoretical model of the response of homogeneous material with completely blocking electrodes. When different physical processes yield response in overlapping frequency regions so that the different processes lead to some melding of effects in an impedance plane representation, interpretation of equivalent circuit parameters becomes difficult even when the degree of fit of the model to the data is excellent. In particular, low frequency extrapolation in the impedance plane to obtain an estimate of bulk resistance, R_b , in an overlapping completely blocking situation can yield estimates of R_b with very large errors. A method is described of avoiding such errors for both conventional and complex least squares estimation. In essence, one must find and fit the unique equivalent circuit whose elements remain related by invariant formulas to underlying microscopic parameters of the material/electrode system no matter what the degree of phenomena overlap.

Small-signal a-c impedance measurements are gaining in popularity as a technique for characterizing liquid and solid electrolytes and other materials. Analysis of small-signal data can almost always yield estimates of bulk conductivity of new materials free from the electrode polarization effects which plague steady-state d-c measurements. Under favorable conditions, detailed analysis of impedance data for homogeneous materials in terms of an appropriate model of the electrode/material system can also yield accurate estimates of microscopic parameters: mobilities, dielectric constant, electrode reaction rate constants, etc., which characterize interface and bulk behavior of the system (1-3). Even for polycrystalline materials, such as the usual form of the superionic conductor β -alumina, proper analysis may lead to valuable information about electrode reactions and intergrain and intragrain properties.

In order to carry out a meaningful analysis of impedance or admittance data, one must compare them with an analytic expression for the measured quantity, a function of frequency which generally depends on several frequency-independent parameters. Optimum characterization of the system requires that one be able to relate the gross parameters of the analytical fitting model to the microscopic parameters of interest. Sometimes, however, in the absence of a sufficiently detailed model one must be satisfied, at least for a while, with estimates of the gross parameter values, since they, and the form of the impedance expression, at least provide a concise means of representing the data. The dependence of the gross parameters, determined from several data sets, on experimental variables such as temperature may then lead to valuable insights.

It is conventional, and very desirable when possible, to approximate the analytical model of the system by an equivalent electrical circuit, preferably one which offers a useful compromise between simplicity and accuracy. It is desirable, for instance, that the equivalent circuit include as few frequency-dependent elements,

such as Warburg (diffusion) impedances (1, 3), as possible. Although the basic analysis method described and illustrated herein does not require equivalent circuit representation, but only an analytical expression of the model, equivalent circuits can often clarify model behavior by clearly identifying separate phenomena which may be significant in quite different frequency ranges. Thus, most of the subsequent analysis herein will employ equivalent circuit representation. Figure 1 is a diagram which illustrates some of the important elements in the characterization process.

Once one has obtained impedance-frequency data, there are three reasonable things one can do. One can plot the impedance, Z , and/or admittance, Y , as a parametric function of frequency in the complex plane (e.g., $\text{Re}(Z)$ along the abscissa and $-\text{Im}(Z)$ along the ordinate axis); one can analyze the data to obtain gross and possibly even microscopic parameters; and one can convert the data to a complex effective dielectric constant, ϵ^*_{eff} , and consider its frequency dependence, loss tangent, and high and low frequency limiting values. The first two approaches are often desirable; the third may not be. Whenever a system involves inhomogeneities and phase boundaries (e.g., homogeneous material and electrodes or polycrystalline material with

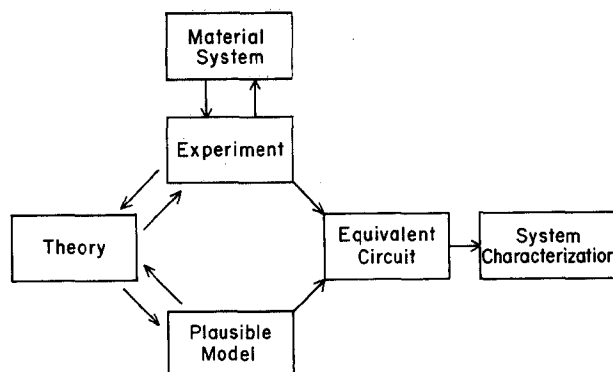


Fig. 1. Block diagram of possible system characterization elements and interactions.

* Electrochemical Society Active Member.

¹ Present address: Department of Geosciences, North Carolina State University, Raleigh, North Carolina 27607.

Key words: complex least squares, data analysis, solid electrolyte, impedance.

or without electrodes), there is a good possibility that these inhomogeneities and phase boundaries may contribute appreciably to the small-signal electrical response of the system. The derivation of an effective dielectric constant for the whole system is then undesirable since dielectric constant is properly defined in terms of an average over a possibly small but macroscopic region of a homogeneous material. Thus, the derivation of a complex dielectric constant and construction of the corresponding Cole-Cole (4) plot is appropriate for a dipolar dielectric with no mobile charge and thus no electrode space-charge or reaction effects, but both are inappropriate when mobile charge is present and electrode and/or grain boundary processes may be important. In this latter case, however, it has been found that plotting the analog of the Cole-Cole diagram, the impedance and/or possibly the admittance, in the complex plane is almost always instructive and useful (1, 3, 5, 6).

Perhaps the most subtle and difficult aspect of impedance data analysis is the development of an adequate analytical model. Some aspects of the general problem of discriminating between several models (*i.e.*, picking the most appropriate one) have been discussed elsewhere (7). One possible model (to be denoted model A) which may be appropriate for the small-signal response over a considerable range of conditions is based on the exact solution of the appropriate transport, continuity, and boundary-condition equations for intrinsic-extrinsic conduction and possible electrode reactions and adsorption (2, 8). It is particularly pertinent for conduction by ions and/or vacancies and interstitials. Some of its predictions for a simple situation are used later in this work to illustrate the analysis method described herein and to demonstrate some pitfalls in interpretation.

The present paper deals primarily with data analysis when an analytical model is available, rather than with the much more difficult problem of finding the best model. Given the model (expressed, say, as an equivalent circuit), how can one best find meaningful estimates of its parameters? One approach, recently employed by de Levie and Vukadin (9), involves a sequence of extrapolations and subtractions. As these authors point out, however, the extrapolation-subtraction method inevitably tends to accumulate (estimation) errors in the last-determined parameters, and it yields no estimates of parameter or fitting uncertainties. It would, therefore, be valuable to have a method that avoids these weaknesses. Such a method is described and illustrated below.

Complex Least Squares

When an analytic expression of a model is available, whether expressed in equivalent circuit form or not, it seems natural to consider least squares fitting of the impedance or admittance data to the impedance or admittance of the selected model in order to obtain estimates of the model parameter values. Several good nonlinear least squares (NLS) computer programs are available which allow fitting of real data to the model $y = f(x)$, with or without weighting of Y_i measured values. Some generalized NLS programs also allow weighting of X_i data values as well (10, 11). Impedance data and analytic expressions are of the form $Z(\omega) = \text{Re}[Z] + i\text{Im}(Z) \equiv u(\omega) + iv(\omega)$. Clearly, $u(\omega)$ and $v(\omega)$ will be different functions of ω but will generally both involve some or all of the same parameters. When complex data have been fitted by least squares in the past, the real $u(\omega)$ and $v(\omega)$ functions have usually been fitted separately using $\text{Re}(Z)$ and $\text{Im}(Z)$ data, respectively. The result of the two independent fittings is then two separate sets of different parameter value estimates.

Although the above type of fitting may be useful, it is not a simultaneous (consistent) least squares fitting of all the data, yielding one set of parameter estimates

determined by all the available data taken together. Therefore, it is desirable to fit the real and imaginary parts of measured impedance to the analytical form of a model or circuit simultaneously. The only published approach of this kind known to the authors is that of Sheppard, Jordan, and Grant (12, 13). We have found, however, that the readily available generalized NLS fitting programs of Powell and Macdonald (10) and Britt and Luecke (11) may be modified very simply to allow fitting of complex data to complex functions. These modified programs seem preferable to the approach outlined by Sheppard (13).

To do complex least squares fitting with the above programs it is unnecessary to use the full theoretical analysis of Britt and Luecke, which involves an arbitrary number of different variables, any of which can be weighted, and which has not been embodied in an actual computer program in complete generality. For typical impedance or admittance data, the measured real and imaginary parts are generally uncertain, and the individual data values may need weighting to obtain the most significant statistical parameter estimates. But the frequency, f or ω , is generally measured so accurately that its uncertainties are negligible. It can then be identified with the x variable, assumed known exactly, in $y = f(x)$ real NLS fitting. Now fitting of complex data, $Z(\omega)$, can be simply reduced, as follows, to real fitting of the usual $y_i = f(x) = f(\omega_i, A_j)$ model form. Here $i = 1, 2, \dots, n$ designates the n complex (double-valued) data points and the n real frequencies, and $j = 1, 2, \dots, m$ denotes the m real parameters, A_j . Let us define y_k as a composite variable with $k = 1, 2, \dots, 2n$. For $k = 1$ to n , let $Y_k \equiv \text{Re}[Z(\omega_k)]$, and for $k = n + 1$ to $2n$, let $Y_k \equiv \text{Im}[Z(\omega_{k-n})]$, where $\text{Re}[Z]$ and $\text{Im}[Z]$ are the real and imaginary measured values of Z . Now, define the analytic fitting model for impedance as $Z_m(\omega_i, A_j) \equiv u(\omega_i, A_j) + iv(\omega_i, A_j)$. The actual analytical separation of the complex Z_m function into real and imaginary parts is unnecessary; only numerical separation by the computer is needed. Thus, we let $u \equiv \text{Re}(Z_m)$ and $v \equiv \text{Im}(Z_m)$ be either analytical or numerical real and imaginary parts of Z_m , and let $y_k \equiv u(\omega_k, A_j)$ for $k = 1$ to n , and $y_k \equiv v(\omega_{k-n}, A_j)$ for $k = n + 1$ to $2n$. Fitting of complex data then just involves the ordinary, real NLS fitting of the real, composite Y_k data ($k = 1$ to $2n$) to the real, composite y_k model (here made up sequentially of the real and imaginary parts of the original complex model). Notice that, unlike ordinary real NLS, one is using different fitting models for the two major parts of the data. This leads to no difficulty in fitting. Since the sum of squares which is minimized by the procedure, is for unity weighting

$$S = \sum_{k=1}^{2n} [Y_k - y_k]^2 = \sum_{i=1}^n [(\Delta R_i)^2 + (\Delta I_i)^2]$$

where ΔR_i and ΔI_i are the real and imaginary fitting residuals, it is evident that we are minimizing the sum of squares of the $s_i = [(\Delta R_i)^2 + (\Delta I_i)^2]^{1/2}$, themselves the distances in the complex plane between a theoretical point and a measured data point, just as desired. Further, as we shall illustrate later, weighting of the $(Y_k - y_k)^2$ squared residuals may be introduced in the usual way. It is also worth noting that the NLS programs of Ref. (10) and (11) require no analytical expressions for function derivatives, a substantial blessing when the model expression is complicated.

The above kind of fitting yields parameter value estimates, estimates of their uncertainties, and an estimate of the standard deviation of fit, s_f . If the data determine some parameter values less precisely than others, this is immediately obvious. Further, s_f may be used to discriminate between various different possible models or equivalent circuits. We suggest that in the past the absence of such a s_f estimate has led to a proliferation of apparently different equivalent cir-

uits not justified by the data themselves. Proper procedure should generally involve choosing that circuit or model which is best justified microscopically and which yields a minimum or at least acceptably small s_f .

Experimental Data: Fitting and Discussion

As an example of complex least squares fitting, we shall analyze the data (private communication) of Hooper, McGeehin, and Hughes (14) on polycrystalline β -alumina with silver electrodes. The 38°C data consist of twelve admittance values spanning the range from 1 kHz to 2 MHz. The corresponding impedance plane plot is shown in Fig. 2. Hooper *et al.* analyzed their data by the extrapolation method using a model equivalent to the three-time-constant Voigt circuit

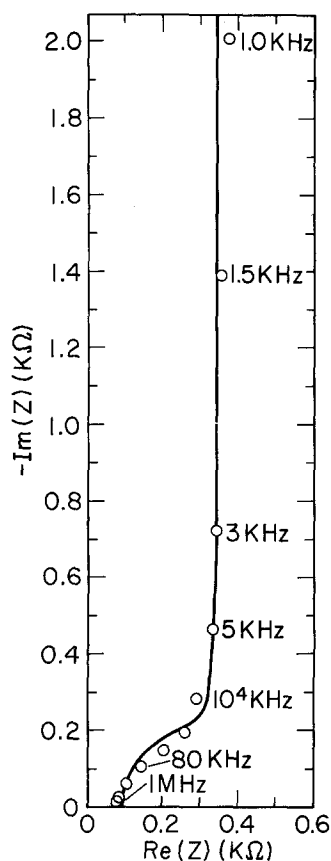


Fig. 2. Impedance plane plot of data (14) for polycrystalline β -alumina at 38°C. Experimental points, least squares line.

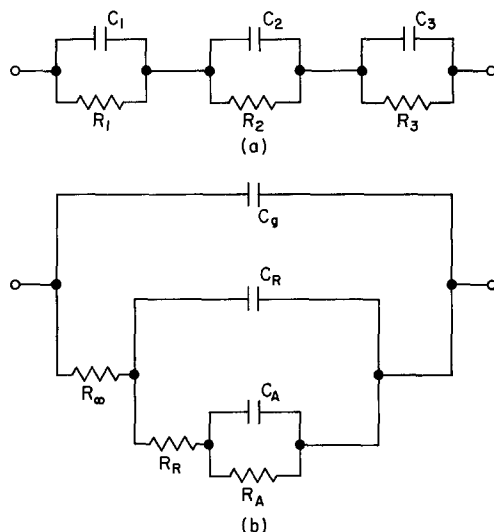


Fig. 3. Possible equivalent circuits for homogeneous and polycrystalline material/electrode systems.

(5, 6) of Fig. 3a with $C_1 = 0$ and $R_2 = \infty$. Before considering a model for least squares fitting and specific fitting results, it is useful to discuss the circuits of Fig. 3 briefly.

First, it has been shown using the exact model A results that the Fig. 3a circuit, which involves no Warburg elements, is appropriate for a homogeneous material when either the positive or the negative mobile species has a much higher mobility than the other, and pertinent time constants are separated from each other by factors of a hundred or more (2, 6). In this loosely coupled case, one can then identify R_1 and C_1 with, respectively, R_z , the unperturbed bulk resistance of the material, and C_g , its geometric capacitance, which is, per unit area, $\epsilon/4\pi l$. Here ϵ is the bulk dielectric constant and l the electrode separation. In addition, R_2 and C_2 may be identified with the electrode reaction resistance R_R and capacitance C_R , and R_3 and C_3 with an adsorption resistance R_A and capacitance C_A . It is assumed that the reaction and adsorption processes, if present, involve the high mobility species with the one of opposite charge completely blocked at the electrodes. The reaction capacitance C_R is often found to be very nearly the double layer capacitance, C_{dl} , of two diffuse space charge layers in series, one from each electrode for identical plane parallel electrodes. Some of the possibilities following from the above are summarized in rows A-D of Table I. Note that complete blocking can occur with either R_2 or R_3 open circuited. Recent work (2) has demonstrated that for the same high mobility ratio situation discussed above, the circuit of Fig. 3b applies exceptionally well for any ratios of the time constants, *i.e.*, for strong as well as weak coupling of the phenomena. It is therefore preferable to that of Fig. 3a for homogeneous material. Note that for loose coupling both circuits lead to three distinct, joined semicircles when impedance is plotted in the complex plane (1, 6). When a resistance is infinite, the corresponding semicircle has infinite radius.

Rows E and F apply to situations involving polycrystalline material between plane, parallel electrodes. It is assumed that the circuit of Fig. 3a is still formally applicable for such material. The bulk properties of all individual grains or crystallites contribute directly to give the over-all effective R_z and C_g . Because of differing grain sizes and orientations, one often finds, when measurements can be extended to sufficiently high frequencies, that the bulk semicircle in the complex impedance plane is displaced downward so that its center lies below the real axis. The R_R , C_R subcircuit, if present, may again be identified with electrode reaction/double layer effects, averaged over crystallites near the electrodes. One frequently finds nearly complete blocking again, as in system E. Farrington (15) has pointed out that adsorbed H_2O or H_2 may be expected to reduce the range over which complete blocking behavior occurs in Na- β -alumina with platinum electrodes. Finally, R_{GB} and C_{GB} are the over-all grain boundary resistance and capacitance associated with the contacts between all individual grains. As usual, one expects $R_z \propto l^2$, $C_g \propto l^{-1}$, and R_R and C_R independent of l , as expected for interface-related quantities. Experiment often suggests that $R_{GB} \propto l^2$ and

Table I. Identification of the R_i , C_i elements of a 6-element Voigt circuit for various systems with loose coupling. Rows A-D apply for homogeneous material and E and F for polycrystalline material.

System	Subcircuit 1		Subcircuit 2		Subcircuit 3	
	R_1	C_1	R_2	C_2	R_3	C_3
A	R_∞	C_g	∞	C_{dl}	—	—
B	R_∞	C_g	R_R	$C_R \equiv C_{dl}$	—	—
C	R_∞	C_g	R_R	$C_R \equiv C_{dl}$	∞	C_A
D	R_∞	C_g	R_R	$C_R \equiv C_{dl}$	R_A	C_A
E	R_∞	C_g	∞	C_R	R_{GB}	C_{GB}
F	R_∞	C_g	R_R	C_R	R_{GB}	C_{GB}

$C_{GB} \propto l^{-1}$, showing these elements to exhibit bulk dependence, as one might perhaps expect for a large number of crystallites arranged in a series-parallel connection with series connections dominating. Here again, one would expect that the grain-boundary semicircle in the impedance plane would be displaced downward more often than not because of the distributed nature of the causes leading to the over-all behavior. Of course, when a semicircle is displaced, it cannot be represented adequately by means of frequency-independent elements such as the R_{GB} and C_{GB} of rows E and F. A more complicated contribution to the total impedance expression must then be employed [e.g., see Ref. (6)], but again one whose parameters can best be estimated by complex least squares fitting.

Some preliminary computer modeling of the electrical properties of grains in series has been carried out by Armstrong, Dickinson, and Willis (16). It involves blocking electrodes, does not show downward displacement of semicircles, and the results appear to be representable by the circuit of row E. Further discussion of grain boundary and intragrain effects in polycrystalline β -alumina has been presented by Powers and Mitoff (17) and by Will (18). Powers and Mitoff give an equivalent circuit which agrees with that of row F except with C_g neglected and (implicitly) with little or no electrode blocking effects, so that $R_R \simeq 0$. Although specific adsorption at an electrode has not been incorporated in the circuits for systems E and F, it may sometimes be of importance and may even be the dominant process leading to nearly complete blocking behavior. Displaced semicircles and nonideal blocking and Warburg-like behavior have been recently reported for polycrystalline lithium silicates and aluminosilicates (19).

The analysis of displaced semicircles and nonideal Warburg-like data behavior in Ref. (19) employs an admittance or impedance function which can be represented by an equivalent circuit with frequency-dependent elements. Unfortunately, this particular approach, which corresponds closely to that of Jonscher in the dielectric area (20), was long ago shown to involve an impedance function associated with a physically nonrealizable system (21). The particular impedance functions used in Ref. (19) and (20) may, nevertheless, be useful empirical fitting functions if not pushed beyond their limits. On the other hand, other, somewhat empirical impedance functions have been proposed (6) which are associated with physically realizable systems, involve frequency-dependent circuit elements, and may be used to represent displaced semicircles and nonideal Warburg behavior. Although they may be formally interpreted in terms of distributions of relaxation times, they are not derived from a detailed microscopic theory of system response and, like all such semiempirical approaches, do not allow direct interpretation of impedance function parameters in terms of specific material parameters such as mobilities, reaction rates, etc. Until a theory which directly leads to nonideal behavior becomes available, circuit element characterization can only be adequately carried out for experiments which yield semicircles with little or no displacement and diffusional response close to ideal, finite-length Warburg behavior (2, 3, 6).

In β -alumina one expects to find many mobile Na^+ ions moving against a background of essentially immobile negative charges. Thus the circuits of Fig. 3 are possibly applicable for single crystal material and, with the interpretations given in rows E and F of Table I, are worth considering for polycrystalline material as well. The data of Hooper *et al.* do not extend to high enough frequencies to allow an estimate to be made of $C_1 \cong C_g$. It may be taken in the least squares fitting as fixed, indifferently, at 0 or at the value calculated from known values of area, ϵ , and l . As mentioned, Hooper *et al.* (implicitly) took $C_1 = 0$, $R_2 = \infty$, and identified R_1 and R_∞ (but including a tortuosity factor),

C_2 with C_{dl} , and R_3 and C_3 with R_{GB} and C_{GB} , essentially row E of Table I with $C_1 = 0$. Since the R_{GB} , C_{GB} semicircle in Fig. 2 is not completely distinct from the C_R rise at low frequencies, it is not clear that the processes are well enough separated that the Fig. 3a circuit should necessarily be used in preference to one like Fig. 3b in interpreting the data (see later discussion). Thus, it is of interest to try fitting the data in impedance form to both the Fig. 3a circuit and that of Fig. 3b. In the latter case, since element identification is uncertain for polycrystalline data (especially where no experiments with different l 's have been carried out), we shall beg the question by letting $C_g \rightarrow 0$, $R_\infty \rightarrow R_1$, $C_R \rightarrow C_2$, $R_R \rightarrow R_2$, $C_A \rightarrow C_3$, and $R_A \rightarrow R_3 \rightarrow \infty$.

The Fig. 3 impedance expressions for fitting are then

$$Z(\omega) = R_1 + (i\omega C_2)^{-1} + [R_3 / (1 + i\omega R_3 C_3)] \quad [1]$$

for Fig. 3a, and

$$Z(\omega) = R_1 + \frac{1 + i\omega R_2 C_3}{(i\omega)[C_3 + C_2(1 + i\omega R_2 C_3)]} \quad [2]$$

for Fig. 3b. Fitting results yield $s_f = 15.98\Omega$ for both fits, carried out with the fixed values $C_1 = 0$ and with $R_2 = \infty$ for the first and $R_3 = \infty$ for the second. For Fig. 3a, one finds $R_1 = (96.5 \pm 7.1)\Omega$, $C_2 = (0.07734 \pm 0.00048)\mu f$, $R_3 = (248.4 \pm 9.3)\Omega$, and $C_3 = (0.0208 \pm 0.0020)\mu f$. Results for the Fig. 3b circuit were $R_1 = (96.5 \pm 7.1)\Omega$, $R_2 = (400.2 \pm 9.3)\Omega$, $C_2 = (0.0164 \pm 0.0020)\mu f$, and $C_3 = (0.06093 \pm 0.00048)\mu f$. If some of the fitting conclusions discussed in the next section apply to the present situation where different processes are not well separated in frequency, the Fig. 3b circuit element values may be more meaningful than the Fig. 3a ones. We shall not, however, pursue this subject further here.

The solid line in Fig. 2 has been drawn from the results of these fittings. It is because both circuits can, with proper element choices, represent the same impedance at all frequencies, as discussed in the next section, that fittings with them yield the same residuals and s_f values. The R_1 element, which is certainly the bulk resistance with crystallite-orientation tortuosity effects included, as stated by Hooper *et al.*, leads to a $38^\circ C$ effective conductivity of about $0.00072 \Omega^{-1} \text{ cm}^{-1}$ using (private communication) $A \cong 0.44 \text{ cm}^2$ and $l \cong 0.3 \text{ cm}$.

While it seems reasonable to identify the R_3 and C_3 elements of Fig. 3a with R_{GB} and C_{GB} , it is clear that C_2 cannot be an ordinary diffuse double layer capacitance. Here $C_2 \simeq 0.176 \mu f/\text{cm}^2$ on a unit electrode area basis, a value very much smaller than would be expected if diffuse double layer theory applied to this very high Na^+ concentration situation. But diffuse layer theory ignores the finite size of charge carriers and discreteness of charge effects. Because of these effects there is a limit to how large the interfacial capacitance (without adsorption) can be (2, 22, 23), although the limit is much larger than the above value of C_2 . While it is clear that C_2 is associated with the blocking character of the material/electrode interface, it is not clear from the present results whether it is an ordinary interface capacitance or is associated with pure specific adsorption (i.e., $R_A \simeq \infty$ in Fig. 3b).

It will be noted that the low frequency points in Fig. 2 do not fall exactly on a vertical line. There are several sources which may lead to such a result, among which are surface roughness (16), specific adsorption (24), recombination (25), and large (but not too large) differences between the mobilities of mobile positive and negative species (1). Although a better fit of the data could be achieved were some of these effects included, possibly with the R_{GB} , C_{GB} circuit also replaced by one with a distribution of time constants (6), we are here more interested in demonstrating a fitting method and discussing the interpretation of the results than in trying to find the best model for the phenomena. In the next section, we consider in further detail

some simple fitting models for homogeneous materials and interpretation of fitting results when synthetic data are employed.

Theoretical "Data:" Fitting and Discussion

Theoretical model.—Some useful conclusions about fitting approaches and parameter interpretation can be developed by consideration and fitting of "data" derived theoretically from a known model. For present purposes it will be sufficient to use the model A already mentioned in its simplest form: an intrinsic situation where positive and negative charges have equal valences, z_e , and mobilities, μ_e ; both are completely blocked at the electrodes; and there is no adsorption. Then R_e (per unit area) becomes $l/(ez_e\mu_e c_i)$, where c_i is the common equilibrium value of the positive and negative charge concentrations, and the Debye length L_D reduces to $[\epsilon kT/8\pi c_i (ez_e)^2]^{1/2}$. It will be convenient to deal with normalized quantities. Let $\tau_D \equiv R_e C_g$, the dielectric relaxation time, $\Omega \equiv \omega \tau_D$, a normalized frequency, and $M \equiv l/2L_D$. Further, normalize impedances and resistances with R_e and capacitances with C_g . Such normalization will be denoted by a subscript "N". In most experimental situations of interest for small-signal impedance measurements, $\Omega \lesssim 1$ and $M \gg 1$.

For the situation defined above, the normalized total impedance of the system turns out to be (1)

$$Z_{TN} = \frac{1 + i\Omega\gamma_1}{i\Omega(1 + i\Omega)\gamma_1} = (1 + i\Omega)^{-1} - [i\Omega(1 + i\Omega)\gamma_1]^{-1} \\ \equiv R_{SN} + (i\Omega C_{SN})^{-1} \quad [3]$$

where $\gamma_1 \equiv M(1 + i\Omega)^{1/2} \text{ctnh}[M(1 + i\Omega)^{1/2}]$. The presence of $(1 + i\Omega)^{1/2}$ and the ctnh function are indications of the distributed nature of the system, consonant with the fact that all real systems are distributed. Their presence also means that no equivalent circuit made up only of frequency-independent circuit elements can represent the impedance of the system exactly. We shall, however, investigate the adequacy of such frequency-independent circuit approximations. Note that in normalized form, the model depends only on the single parameter M . Let us use a subscript zero to denote the limit $\Omega \rightarrow 0$. Then one finds (8) that $R_{SNO} = 1 + \{[r - 2 + \{(M) \text{csch}(M)\}^2]/2(r - 1)^2\}$ and $C_{SNO} = r - 1$, where $\gamma_{10} \equiv r \equiv (M) \text{ctnh}(M)$. For $M \gg 1$, $R_{SNO} \approx 1 + (2M)^{-1} \approx 1$. The total low frequency-limiting normalized parallel capacitance is $C_{PNO} = C_{SNO} + C_{gN} = r$. This result reduces to just the ordinary specific diffuse double layer capacitance for two double layers in series, one near each of the two identical electrodes, $C_{P0} = \epsilon/8\pi L_D$, for $M \gg 1$.

Circuits and curves.—For the present system, the circuits of Fig. 3a and 3b reduce, respectively, to essentially those of Fig. 4a and 4c. We shall investigate the

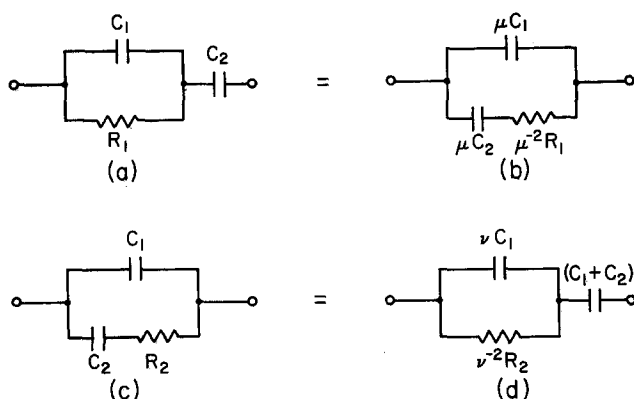


Fig. 4. Lumped-constant equivalent circuits with equal impedances when circuit (a) values are used to form $\mu \equiv C_2/(C_1 + C_2)$ and circuit (c) values are employed to form $\nu \equiv (C_1 + C_2)/C_2$.

applicability of these circuits and the identity of their elements by NLS fitting of exact "data" calculated from the Eq. [3] model to the approximate models represented by these equivalent circuits. Although the Fig. 4a circuit has been widely employed for liquid, and to some extent, solid electrolyte situations, it will prove less directly applicable than that of Fig. 4c for the present homogeneous-material situation. Circuits 4a and 4c are degenerate forms of more complex equivalent circuits known as Voigt and Maxwell circuits, respectively (5, 6). The equality signs in Fig. 4 indicate that these circuits may be made to exhibit exactly the same impedance at all frequencies provided element values are chosen appropriately, as shown in the figure. Thus for example, the circuit of Fig. 4b will have the same impedance as that of 4a if the 4b element values are related, as shown, to those in 4a through the quantity μ , which involves a ratio of 4a capacitance values.

Before considering detailed NLS fitting results, it is of interest to examine impedance and admittance plane plots following from Eq. [3]. Thus Fig. 5 and 6 show complex impedance and admittance plane plots of Z_{TN} and $Y_{TN} \equiv Z_{TN}^{-1}$ as parametric functions of Ω for several M values. As is conventional, we have actually plotted $Z_{TN}^* = \text{Re}[Z_{TN}] - i\text{Im}[Z_{TN}]$ in the (normalized) impedance plane. The $(0,0; 1,1; 0,M)$ designation on the figures specifies completely blocking electrodes, equal valence numbers and mobilities, and no extrinsic conduction character. For $M \gg 10^2$, Fig. 5 shows that there is present a semicircle, which is associated (in unnormalized form) with the bulk parameters C_g and R_e , and a well-distinguished vertical line, associated with the double layer capacitance. When $M \lesssim 10$, however, the bulk semicircle and the diffuse layer line begin to meld together since the frequency ranges where they occur approach each other more and more as M decreases. Qualitatively similar behavior occurs for the admittance plane results, but the semicircle there involves R_e and the double layer capacitance, and the vertical line is associated with C_g .

Were we to use NLS fitting of exact "data" derived from Eq. [3] to the Eq. [3] model itself, one would of course obtain a fit whose accuracy would be limited only by computer round-off error, and would also ob-

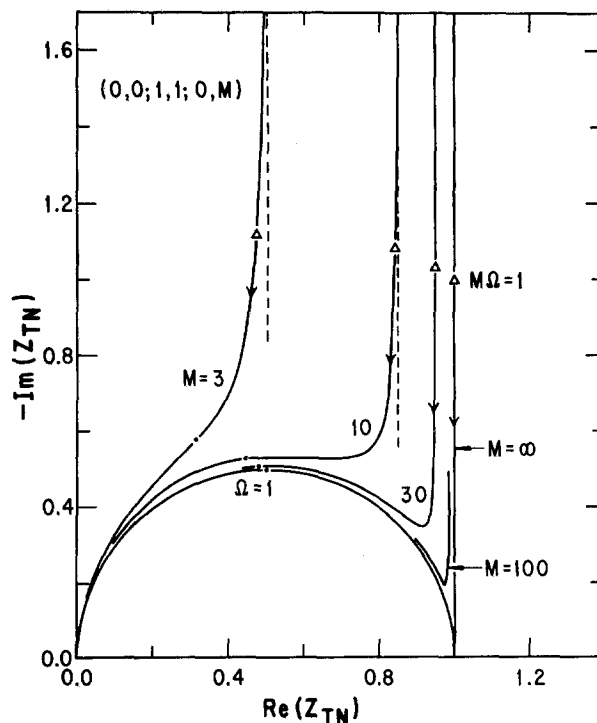


Fig. 5. Complex impedance plane plot of normalized impedance for the $(0,0; 1,1; 0,M)$ situation.

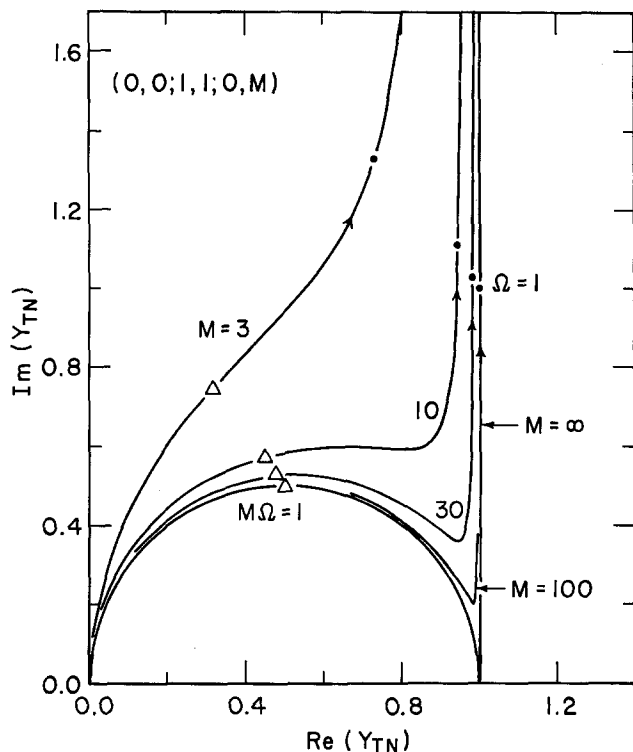


Fig. 6. Complex admittance plane plot of normalized admittance for the (0,0; 1,1; 0,M) situation.

tain a similarly accurate estimate of the single parameter M . In many experimental situations, however, one either does not have a good analytic model for fitting or finds that the appropriate analytic model is too complicated for direct least squares fitting (*i.e.*, model A in full generality). Thus one often finds an equivalent circuit approach to be useful.

Conventional analysis.—Although there is only one parameter, M , in the Z_{TN} of Eq. [3], there are three things which we want to determine from $Z_{TN}(\Omega)$ as accurately as possible. These are the normalized geometric capacitance and bulk resistance, both unity with present normalization, and M or r . If they can be well determined, we are assured that a similar procedure applied to unnormalized $Z_T(\omega)$ data will yield good values of C_g , R_{∞} , and C_{PO} . Since there are three distinct circuit elements in the circuits of Fig. 4a and 4c, one might expect that these elements could be related rather simply to C_g , R_{∞} , and C_{PO} , which are themselves expressed in terms of microscopic parameters. Consider first the usual extrapolation method applied to curves like those in Fig. 5 and 6. There is clearly no problem in obtaining estimates of C_g , R_{∞} , and a frequency-independent double layer capacitance, say C_{dl} , from results such as those in Fig. 5 or 6 when $M \gg 10^2$. Then R_{∞} (here $R_{\infty N} = 1$) may be obtained directly from the real-axis intercept of the vertical line in Fig. 5, C_{dl} from the capacitive reactance of a point on the line, and C_g from a point on the semicircle. Similarly, in Fig. 6, G_{∞} (or $G_{\infty N} = 1$ here) occurs at the real axis intercept of the vertical line, C_g may be derived from the reactance on the line, and C_{dl} from a point on the admittance-plane semicircle.

Unfortunately, the situation is not so clear for relatively small M . Some authors have nevertheless used the extrapolation to the real axis of the asymptote of a curve such as that for $M = 3$ or 10 in Fig. 5 to obtain an estimate for R_{∞} . An extrapolation of this kind appears, for example, in Ref. (19). As Fig. 5 shows, such extrapolation can yield an R_{∞} estimate incorrect by a factor of two or more for the present situation. In Fig. 6, on the other hand, all curves approach the $\text{Re}(Y_{TN}) = 1$ line asymptotically, but this is by no means clear from that portion of the $M = 3$ curve shown, which

might correspond to as much of an experimental curve as could be measured conveniently in a specific instance.

The determination of R_{∞} from the real axis intercept of a vertical line associated with completely blocking electrode behavior corresponds to estimating R_{∞} from low frequency experimental data since the impedance-plane vertical line occurs at the lowest frequencies of measurement. Alternatively, unlike such low frequency extrapolation, the determination of G_{∞} from the real axis intercept of a vertical straight line in the admittance plane corresponds to high frequency extrapolation, and is in keeping with the $\omega \rightarrow \infty$ subscript of G_{∞} , the only conductance one expects to remain significant at sufficiently high frequencies. Similarly, C_{dl} is estimated by a low frequency extrapolation of Z_T data and C_g by a high frequency extrapolation of Y_T data. Although it is indeed much more common in liquid electrolyte work to obtain an R_{∞} estimate from high rather than from low frequency extrapolation, Rais-trick, Ho, and Huggins (19) have pointed out that for solid electrolytes practical frequency-range limitations often require R_{∞} estimation by low frequency extrapolation (as in Fig. 5) for results obtained at low temperatures. We shall shortly demonstrate how such an estimate, which may differ appreciably from the true R_{∞} , may be transformed to obtain a much more appropriate estimate of R_{∞} .

Comparison of the shapes of the Fig. 2 curve for β -alumina and that for $M = 3$ of Fig. 5 shows considerable likeness. Since we have already seen that an extrapolation of the Fig. 5 $M = 3$ vertical asymptote to the real axis yields $R_{\infty N} \approx 0.5$ instead of the correct unity value, it is reasonable to conclude that in the case of Fig. 2, which also displays overlapping of phenomena, similar extrapolation may again lead to considerable error. Whenever this error cannot be reduced by high frequency extrapolation (because such data are lacking), it turns out, nevertheless, that it can be reduced by proper interpretation. But, as we shall see, NLS fitting of an appropriate model will always yield the most significant estimates of parameter values.

NLS analysis.—The theoretical "exact data," calculated with double precision on an IBM 370-155 computer from Eq. [3] for $M = 10^4, 30$, and 3, consisted of 25 complex Z_{TN} or Y_{TN} values and 25 Ω values. The Ω values were uniformly distributed in $\log \Omega$ and covered $10^{-5} \leq \Omega \leq 10$ for $M = 10^4$ and $10^{-2} \leq \Omega \leq 10$ for $M = 30$ and 3. The data were fitted to the models of circuits of Fig. 4a and 4c

$$Z_{TN} = [R_{1N}/(1 + i\Omega R_{1N}C_{1N})] + (i\Omega C_{2N})^{-1} \quad [4]$$

and

$$Z_{TN} = [i\Omega\{C_{1N} + C_{2N}(1 + i\Omega R_{2N}C_{2N})^{-1}\}]^{-1} \quad [5]$$

respectively, with double-precision arithmetic using the present complex NLS method.

Results of fitting exact Z_{TN} "data" to the Eq. [5] model for Z_{TN} are shown in the first line of Table II for each M value. The second line presents the results of fitting exact $Y_{TN} \equiv Z_{TN}^{-1}$ "data" to the Y_{TN} following from Eq. [5]. If we identify C_{1N} as an estimator of $C_{gN} = 1$, R_{2N} as the R_{SNO} defined earlier, and C_{2N} as C_{SNO} , then the expected values of these quantities are as shown in the third line for each M choice. It is evident that these identifications are reasonable.

The \pm quantities shown in the table are estimated relative standard deviations of the parameters. Had the circuit model been exactly appropriate for the data, the relative standard deviations would have arisen only from round-off error and would have been of the order of 10^{-12} or less in the present calculations. The larger values apparent here are a measure of the inexactness of the circuits employed. The larger M , clearly the better the lumped-constant approximations are to the actual distributed system. If one judged from the overall estimated standard deviation of the fit, s_f , one might

Table II. Fitting of unweighted (0,0; 1,1; 0,M) "data" to the circuit of Fig. 4c. For each M value: first line Z_{TN} fitting; second line $Y_{TN} \equiv Z_{TN}^{-1}$ fitting; third line expected value

M	Standard deviation of fit, s_f	C_{1N}	R_{2N}	C_{2N}
10 ⁴	6.6 × 10 ⁻⁷ 6.0 × 10 ⁻⁶	1.000009 (1 ± 7.1 × 10 ⁻⁷) 1.000002 (1 ± 4.9 × 10 ⁻⁷)	1.0000498 (1 ± 1.5 × 10 ⁻⁷) 1.0000457 (1 ± 1.3 × 10 ⁻⁶)	9.999000 × 10 ⁸ (1 ± 5.5 × 10 ⁻⁸) 9.999000 × 10 ⁸ (1 ± 6.6 × 10 ⁻⁶)
30	2.9 × 10 ⁻⁴ 2.3 × 10 ⁻³	1.00295 (1 ± 2.2 × 10 ⁻⁴) 1.00076 (1 ± 1.5 × 10 ⁻⁴)	1.01669 (1 ± 8.0 × 10 ⁻⁵) 1.01396 (1 ± 5.3 × 10 ⁻⁴)	28.9965 (1 ± 5.9 × 10 ⁻⁶) 28.9759 (1 ± 1.8 × 10 ⁻⁸)
3	7.2 × 10 ⁻⁴ 9.1 × 10 ⁻³	1.0128 (1 ± 7.2 × 10 ⁻⁴) 1.0050 (1 ± 6.2 × 10 ⁻⁴)	1.1500 (1 ± 8.1 × 10 ⁻⁴) 1.1136 (1 ± 3.4 × 10 ⁻⁸) 1.13603776	2.0021 (1 ± 3.6 × 10 ⁻⁴) 1.9818 (1 ± 7.9 × 10 ⁻⁸) 2.0149094698

conclude that even for M as small as 3, the lumped-constant approximation would be adequate except for the most accurate data. One must, however, consider the estimated values of the parameters themselves and must treat all standard deviations shown here with caution. Since differences between the exact result of Eq. [3] and the present circuit models are systematic rather than random in nature, the least squares fitting residuals will generally show systematic behavior and will not be randomly distributed. The standard deviations will then generally be poor approximations (usually too small) although their trends here are certainly significant.

The results of Table II show that the circuit of Fig. 4c is indeed a good approximate model for the present system. It is also evident, in accordance with the conclusions of conventional analysis discussed above, that C_{1N} is best estimated from Y_{TN} fitting and R_{2N} and C_{2N} from Z_{TN} fitting. Although the differences here are associated with systematic errors, it is likely that the same conclusions will apply to experimental data dominated by random rather than systematic errors.

For $M \gtrsim 30$, the Table II results show that the parameter estimates are highly accurate. Even the $M = 3$ results are likely to be generally adequate. But how would one proceed to obtain estimates of M , C_g , and R_x if these quantities were unknown and one were analyzing experimental, unnormalized data? Let us consider the worst case here, $M = 3$, and deal with the present results as actually derived from unnormalized data, i.e., that for which true M , C_g , and R_x values are 3, 1, and 1, respectively, in appropriate units. Assume further that only the $Z_{TN} \rightarrow Z_T$ fitting results are available. Then an estimate of r is $1 + (C_2/C_1) = 1 + (2.0021/1.0128) \cong 2.9768$ and the corresponding M estimate is 2.9609, in error by about 1%. The $C_1 = 1.0128$ estimate of C_g is also about 1% in error. The above values of r and M now allow one to calculate R_{SNO} , yielding 1.13708 (instead of the correct 1.13604). Then an estimate of R_x is $R_x \cong R_2/R_{SNO} = 1.15/1.13708 \cong 1.011$, again in error by about 1%. Thus, even in the

extreme high overlap case of $M = 3$, we are able to use the circuit Fig. 4c model to obtain desired parameters to about 1%.

Now what happens if exact Z_{TN} "data" is fitted to the circuit Fig. 4a model, Eq. [4]? Some results are shown in Table III. Notice that the s_f values are exactly the same as the corresponding Z_{TN} results in Table II, showing that both circuits can fit the "data" to the same degree. But it is evident that C_{1N} here is an appreciably poorer estimate of $C_{gN} = 1$ than the C_{1N} of Table II and that R_{1N} , particularly for small M , is a very poor estimate of either R_{SNO} or $R_{xN} = 1$. On the other hand, C_{2N} is evidently a better estimate of $C_{PNO} = r$ here than is the C_{2N} of Table II of $r = 1$. Finally, it is gratifying to note that when the parameter estimates of Table III, associated with the Fig. 4a circuit, are transformed (by the relations shown in Fig. 4) to parameter values pertaining to the Fig. 4c circuit, one obtains exactly (within round off) the values shown in Table II for all M choices.

These results and conclusions suggest that best estimates of M , C_g , and R_x might be obtained using a C_1 estimate obtained from admittance data fitting of the Fig. 4c circuit, a R_2 estimate from impedance fitting of the Fig. 4c circuit, and a C_2 estimate either from impedance fitting of the Fig. 4a circuit or by transformation of the Fig. 4c impedance fitting results to yield a Fig. 4a C_2 estimate. For most purposes, however, Z_{TN} fitting to the Fig. 4c circuit should be sufficient.

In the present synthetic data situation, we know for the Fig. 4c circuit that C_{1N} , which represents $C_{gN} = 1$, should be unity. Table IV presents some results obtained when C_{1N} is constrained to remain unity during NLS fitting. The first three lines in the table, for unweighted (i.e., unity, weighted) residuals, show that fixing C_{1N} has increased s_f values and most of the parameter relative standard deviations but has generally improved the R_{2N} and C_{2N} estimates appreciably. Moral: use *a priori* information when available.

In some cases, it may be desirable to carry out NLS fitting with weightings different from unity. Consider

Table III. Fitting of unweighted (0,0; 1,1; 0,M) Z_{TN} "data" to the circuit of Fig. 4a

M	Standard deviation of fit, s_f	C_{1N}	R_{1N}	C_{2N}
10 ⁴	6.6 × 10 ⁻⁷	1.0001092 (1 ± 7.1 × 10 ⁻⁷)	0.9998498 (1 ± 1.5 × 10 ⁻⁷)	1.00000000 × 10 ⁴ (1 ± 5.5 × 10 ⁻⁸)
30	2.9 × 10 ⁻⁴	1.03764 (1 ± 2.3 × 10 ⁻⁴)	0.94985 (1 ± 7.8 × 10 ⁻⁶)	29.9945 (1 ± 5.7 × 10 ⁻⁶)
3	7.2 × 10 ⁻⁴	1.5253 (1 ± 1.1 × 10 ⁻⁸)	0.5071 (1 ± 3.6 × 10 ⁻⁴)	3.01490 (1 ± 1.4 × 10 ⁻⁶)

Table IV. Fitting of (0,0; 1,1; 0,M) Z_{TN} "data" to the Fig. 4c circuit with C_{1N} fixed at unity

M	Weighting uncertainty, σ_x	Standard deviation of fit, s_f	R_{2N}	C_{2N}
10 ⁴	1	1.4 × 10 ⁻⁶	1.0000498 (1 ± 3.1 × 10 ⁻⁷)	9.999000 × 10 ⁸ (1 ± 1.2 × 10 ⁻⁷)
30	1	6.2 × 10 ⁻⁴	1.0165 (1 ± 1.6 × 10 ⁻⁴)	28.998 (1 ± 1.3 × 10 ⁻⁴)
3	1	2.0 × 10 ⁻³	1.135 (1 ± 9.8 × 10 ⁻⁴)	2.01485 (1 ± 5.9 × 10 ⁻⁵)
	$\begin{cases} x \\ x^{-1} \\ x^{-2} \\ x^{-4} \end{cases}$	$\begin{cases} 1.0 \times 10^{-3} \\ 1.2 \times 10^{-3} \\ 9.0 \times 10^{-4} \\ 7.7 \times 10^{-4} \end{cases}$	$\begin{cases} 1.130 (1 \pm 2.9 \times 10^{-3}) \\ 1.141 (1 \pm 9.6 \times 10^{-4}) \\ 1.1488 (1 \pm 9.6 \times 10^{-5}) \\ 1.149005 (1 \pm 2.4 \times 10^{-7}) \end{cases}$	$\begin{cases} 2.015 (1 \pm 3.6 \times 10^{-8}) \\ 2.01490 (1 \pm 1.5 \times 10^{-8}) \\ 2.0149093 (1 \pm 6.9 \times 10^{-8}) \\ 2.014909468 (1 \pm 1.4 \times 10^{-10}) \end{cases}$

a datum value x , say the real or imaginary part of an impedance. Let σ_x be the estimated uncertainty of a given x value. Then the appropriate weighting of the squared residual corresponding to this value of x becomes $w_x = \sigma_x^{-2}$. One might know, for example, that small values of x are more uncertain than large values because of limitations in resolution of measuring techniques, etc. Then, one might take, as a first approximation, $\sigma_x = a|x|^{-1}$, where a is a constant. Then $w_x = a^{-2}x^2$, and residuals associated with larger x values are thus more heavily weighted than those associated with smaller x . The last four lines of Table IV show nonunity weighting results for $M = 3$. One notices that $|x|$ weighting is worse than unity weighting and that as weighting progressively emphasizes larger values, R_{2N} estimates degrade and C_{2N} ones improve. This trend is not surprising since at low Ω values the contribution of C_{2N} dominates the expression for Z_{TN} in the present completely blocking situation. Although such extreme weighting as $\sigma_x = |x|^{-4}$ will be inappropriate for actual experimental data, it has here allowed us to estimate C_{SNO} correct to eight or nine decimal places. For experimental situations $|x|^{-1/2}$, or possibly $|x|^{-1}$, weighting may sometimes be useful.

As we have mentioned earlier, it is often impossible or inconvenient to carry out impedance measurements to sufficiently high frequencies to cover most of the bulk-effect semicircle. Here we have indeed done so by extending the data to $\Omega = 10$ ($\omega_{\max} = 10/\tau_D$). Separate fittings with $\Omega_{\max} < 10$ have shown, in fact, that for the present system, parameter estimates are improved if, say, $\Omega_{\max} = 0.1$ rather than 1 or 10. The choice $\Omega_{\max} = 0.1$ is a high enough (normalized) frequency that C_{1N} may still be reliably estimated, but it extends less far into the region where the distributed nature of the system (not represented by our equivalent circuits), appearing through $(1 + i\Omega)^{1/2}$, is more important.

In concluding this section, we suggest that in completely blocking situations the complex NLS fitting of impedance data, extending up to perhaps $\omega_{\max} \sim (10\tau_D)^{-1}$, to the circuit of Fig. 4c is most appropriate for general purpose work. Further, several weightings different from unity should be tried for the above fitting in order to find the weighting(s) which yield(s) minimum estimated standard deviations of the several parameters of interest. Even in nonblocking situations, such weighting investigation should often prove useful.

Effect of length and concentration variation.—The use of normalized quantities, as in Eq. [3] and Fig. 5 and 6, is helpful in allowing one to subsume many possible dependencies in one. Real data are initially unnormalized, however, and it is therefore of interest to examine how unnormalized impedance/admittance-plane curves corresponding to the normalized curves of Fig. 5 and 6 depend on variation of such parameters as electrode separation length and equilibrium charge concentration.

Let us consider two values of length, l_1 and l_2 , and two of concentration, c_{11} and c_{12} . Then one readily finds from the equations and definitions above that for l and c_1 variation alone, $M_2/M_1 = (l_2/l_1)(c_{12}/c_{11})^{1/2}$, and $R_{2,2}/R_{2,1} = (l_2/l_1)(c_{11}/c_{12})$. Further, $\tau_{D2}/\tau_{D1} = (l_2/l_1)^0 (c_{11}/c_{12})$. Since $Z_T \equiv R_x Z_{TN}$ and $Y_T \equiv G_x Y_{TN}$, it is clear that R_x and G_x determine the scales of the unnormalized Z_T and Y_T curves, respectively, following from Z_{TN} and Y_{TN} . Thus, unnormalized curve size may be readily obtained from normalized results when R_x or G_x is known. But complex plane curves are parametric in frequency. Therefore, it is desirable to investigate how frequency points move their position along unnormalized curves as such quantities as l and c_i change. Figures 5 and 6 show two points with normalized frequency $\Omega = 1$ and $M\Omega = 1$. Their positions do not change much until M is considerably less than 100. But suppose we ask how the ω 's involved in $\Omega \equiv \omega\tau_D$ must change as l and c_i change when we restrict

Table V. Effects of l and c_i variation on pertinent quantities

Variation					$\Omega = 1$	$M\Omega = 1$
M_2/M_1	l_2/l_1	c_{12}/c_{11}	$R_{2,2}/R_{2,1}$	$G_{2,2}/G_{2,1}$	ω_2/ω_1	ω_2/ω_1
10	10	1	10	0.1	1	0.1
	1	10^2	10^{-2}	10^2	10^2	10
1	$10^{1/2}$	10	$10^{-1/2}$	$10^{1/2}$	10	1
	0.1	10^2	10^{-2}	10^2	10^2	10^2
	10	10^{-2}	10^2	10^{-2}	10^{-2}	10^{-2}

attention to the same two points $\Omega = 1$ and $M\Omega = 1$ of Fig. 5 and 6. One easily obtains for $\Omega = 1$ the relation $\omega_2/\omega_1 = (l_1/l_2)^0 (c_{12}/c_{11})$, and for $M\Omega = 1$ the result $\omega_2/\omega_1 = (l_1/l_2)(c_{12}/c_{11})^{1/2}$.

The above relations have been employed to calculate the specific results of Table V. It shows the effects of various l and c_i variations which produce $M_2/M_1 = 10$ and 1. We see, for example, that a 10 times increase in l with no change in c_i yields unnormalized impedance plane curves 10 times larger than the normalized ones. No change occurs in the ω corresponding to $\Omega = 1$, but that corresponding to $M\Omega = 1$ occurs at one-tenth the frequency found for the original length. The ω frequency scale is thus not shifted uniformly by a change of length. On the other hand, when l and c_i change in such a way that M remains the same, the results of the bottom two lines in the table show that the frequency scale is then uniformly expanded or contracted.

Acknowledgments

We much appreciate the helpful comments of Dr. D. R. Franceschetti and the kind assistance of Dr. A. Hooper in supplying his β -alumina data for analysis. This work was supported by the U.S. National Science Foundation, Grant No. DMR 75-10739.

Manuscript submitted Dec. 14, 1976; revised manuscript received March 11, 1977.

Any discussion of this paper will appear in a Discussion Section to be published in the June 1978 JOURNAL. All discussions for the June 1978 Discussion Section should be submitted by Feb. 1, 1978.

Publication costs of this article were assisted by the National Science Foundation.

REFERENCES

- J. R. Macdonald, *J. Chem. Phys.*, **61**, 3977 (1974).
- D. R. Franceschetti and J. R. Macdonald, *J. Electroanal. Chem.*, To be published.
- J. R. Macdonald, *ibid.*, **53**, 1 (1974).
- K. S. Cole and R. H. Cole, *J. Chem. Phys.*, **9**, 341 (1941).
- J. R. Macdonald, in "Electrode Processes in Solid State Ionics," M. Kleitz and J. Dupuy, Editors, p. 149, D. Reidel Publishing Co., Dordrecht, Holland (1976).
- J. R. Macdonald, in "Superionic Conductors," G. D. Mahan and W. L. Roth, Editors, p. 81, Plenum Press, New York (1976).
- J. R. Macdonald and D. R. Powell, *J. Res. Nat. Bur. Stand. (U.S.)* **75A**, 441-453 (1971).
- J. R. Macdonald, *J. Chem. Phys.*, **58**, 4982 (1973).
- R. de Levie and D. Vukadin, *J. Electroanal. Chem.*, **62**, 95 (1975).
- D. R. Powell and J. R. Macdonald, *Computer J.*, **15**, 148 (1972).
- H. I. Britt and R. H. Luecke, *Technometrics*, **15**, 233 (1973).
- R. J. Sheppard, B. P. Jordan, and E. H. Grant, *J. Phys. D.*, **3**, 1759 (1970).
- R. J. Sheppard, *ibid.*, **6**, 790 (1973).
- A. Hooper, P. McGeehin, and A. E. Hughes, in "Superionic Conductors," G. D. Mahan and W. L. Roth, Editors, p. 99 (abstract), Plenum Press, New York (1976); Full details in A. Hooper, Report No. AERE-R8412, Harwell; *J. Phys. D.*, To be published.
- G. C. Farrington, *This Journal*, **123**, 833 (1976).
- R. D. Armstrong, T. Dickinson, and P. M. Willis, *J. Electroanal. Chem.*, **53**, 389 (1974).
- R. W. Powers and S. P. Mitoff, *This Journal*, **122**, 226 (1975).

18. F. G. Will, *ibid.*, **123**, 834 (1976).
 19. I. D. Raistrick, C. Ho, and R. A. Huggins, *ibid.*, **123**, 1467 (1976).
 20. A. Jonscher, *Nature* (London), **253**, 717 (1975); *Phys. Status Solidi*, **32**, 665 (1975).
 21. J. R. Macdonald, *Rev. Mod. Phys.*, **28**, 393 (1956); *ibid.*, **28**, 41 (1956).
 22. R. D. Armstrong, *J. Electroanal. Chem.*, **52**, 413 (1974); *ibid.*, **66**, 148 (1975).
 23. J. R. Macdonald, *ibid.*, **66**, 143 (1975).
 24. J. R. Macdonald and P. W. M. Jacobs, *J. Phys. Chem. Sol.*, **37**, 1117 (1976).
 25. J. R. Macdonald, D. R. Franceschetti, and R. Meaudre, *J. Phys. C.*, To be published.

The Kinetics of the Magnesium Electrode in Thionyl Chloride Solutions

E. Peled* and H. Straze

Institute of Chemistry, Tel Aviv University, Ramat Aviv, Tel Aviv, Israel

ABSTRACT

The electrochemical behavior of the magnesium electrode in thionyl chloride (TC) solutions was studied. It was found that this electrode is covered by a passivating layer which consists of some insoluble magnesium salt, probably $MgCl_2$. The properties of this layer determine the chemical and electrochemical behavior of the electrode in TC solutions. Magnesium was deposited on a nickel cathode from TC solutions containing $Mg(FeCl_4)_2$. Magnesium deposition begins after the nickel cathode is covered by a passivating layer (consisting of reduction products of TC) in which $t_{Mg^{2+}} \sim 1$. It was concluded that the rds for the deposition-dissolution process of the magnesium electrode in TC solutions is not the electron-transfer reaction, but is instead the migration of the Mg^{2+} ions through a passivating layer which covers the electrode.

There has been no report in the literature of kinetics of the deposition-dissolution process for solid magnesium metal in nonaqueous solutions. However, many papers have been published in the last fifteen years on the kinetics of alkali metals in these media. The reason for this is that magnesium is a much more difficult metal to electrodeposit than are the alkali metals. Most of the attempts to electrodeposit magnesium from nonaqueous solutions have been unsuccessful (1).

The only system in which the electrodeposition of magnesium is feasible is that of Grignard reagents with the addition of boranes in ether solutions (2).

The electrode kinetics of the alkali metals in propylene carbonate, dimethyl sulfoxide, and dimethyl sulfide is reviewed in Ref. (3-6). Most of the investigations deal with the electrochemical behavior of the lithium electrode. It was found (3-6) that: (i) lithium metal is chemically stable in these solutions, (ii) film formation on the electrode has been detected, (iii) trace amounts of water induce film formation, and (iv) the reaction $Li^+ + e(M) \rightleftharpoons Li$ has a high exchange current density ($1-10 \text{ mA cm}^{-2}$).

The rate-determining step (rds) of the deposition-dissolution process for solid alkali metals was assumed to be the electron-transfer reaction: $M^+ + e(M) \rightleftharpoons M^0$ with a transfer coefficient (α) of 0.5-0.8 (3-6). Dey (7) indicated that in propylene carbonate solutions the lithium electrode is covered by a passive film (probably Li_2CO_3) which is formed by the reaction between lithium and propylene carbonate. He concluded that this film should be a purely ionic conductor with the Li^+ being the sole conducting species ($t_{Li^+} = 1$) (7). The same conclusion was drawn (8) for lithium electrode in thionyl chloride solutions.

In this paper the electrochemical behavior of solid magnesium electrode in thionyl chloride solution was studied. It was found that the rds of the deposition-dissolution process for magnesium metal in thionyl chloride (TC) solution is not the electron-transfer reaction but is the migration of the magnesium ions through a passivating layer which covers the electrode.

Experimental

The cell and the electrodes are shown in Fig. 1. The three electrodes were made from magnesium ribbon BDH 99.9%, 0.4 mm thick and 3 mm wide. The working and reference electrodes were parallel to each other and about 5 mm apart. They had an area of 1.4-2.5 cm^2 . Each electrode was connected by a stainless steel connector to a tungsten rod sealed in the glass cap. The cell was sealed by a Viton O-ring. Connection to the vacuum line was made through a Jobling "Rotaflo" valve. The magnesium electrodes were

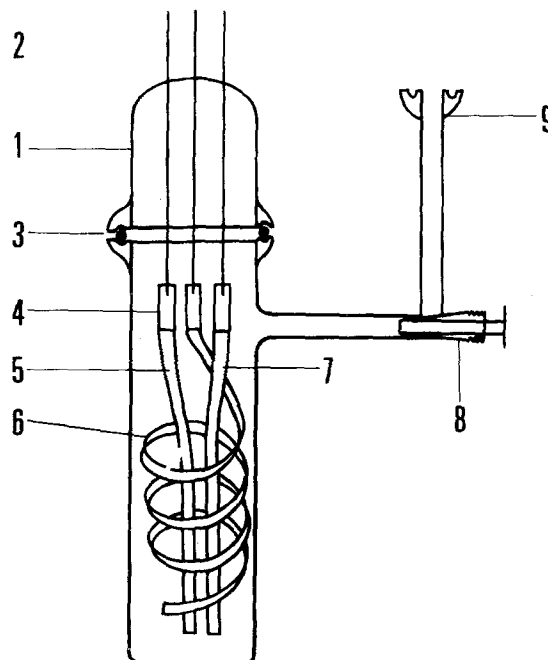


Fig. 1. The electrochemical cell. 1, Cell cap; 2, tungsten wires; 3, Viton O-ring; 4, stainless steel connectors; 5, working electrode; 6, counterelectrode; 7, reference electrode; 8, "Rotaflo" valve; 9, connection to vacuum line.

* Electrochemical Society Active Member.

Key words: passivating layer, magnesium electrodeposition, inorganic battery.